Electronic structure of antidot superlattices in commensurate magnetic fields

2001 J. Phys.: Condens. Matter 13 3365

(http://iopscience.iop.org/0953-8984/13/14/310)

INSTITUTE OF PHYSICS PUBLISHING JOURNAL OF PHYSICS: CONDENSED MATTER

J. Phys.: Condens. Matter **13** (2001) 3365–3379 www.iop.org/Journals/cm PII: S0953-8984(01)20870-4

Electronic structure of antidot superlattices in commensurate magnetic fields

Egidijus Anisimovas[1] **and Peter Johansson**[1,2]

[1] Division of Solid State Theory, Department of Physics, University of Lund, Sölvegatan 14 A, S-223 62 Lund, Sweden
[2] Department of Natural Sciences, University of Örebro, S-701 82 Örebro, Sweden

E-mail: egidijus@teorfys.lu.se (E Anisimovas)

Received 6 March 2001

Abstract

We present a treatment of an interacting two-dimensional electron system moving in a bidirectionally periodic potential and a perpendicular magnetic field. Employing symmetry considerations based on the ray-group of magnetotranslation operators and a canonical coordinate transformation, we derive an efficient scheme for calculating energy levels and states in arbitrary 'rational' magnetic fields. Applying this scheme to a superlattice of strongly localized antidots we reveal the possibility to split off an isolated and sufficiently broad cluster of subbands from a Landau band. The implications of the existence of such subbands to the experimental detection of the subband structure and in particular quantum Hall effect measurements in periodic superlattices are discussed.

1. Introduction

Inspired by advances in submicron technology, there has recently been a considerable amount of both theoretical and experimental work aimed at understanding the physics which governs the behaviour of realistic quasi-two-dimensional electron systems (2DES) subjected to perpendicular magnetic fields and man-made lateral periodic confinements. Such systems have been prepared and investigated covering a wide range of periodic modulation strength. In weakly perturbed 2DES, a main pursuit was the commensurability-related magnetoresistance oscillations [1] explained by the broadening of Landau levels into bands. When the superlattice potential is applied in both lateral directions [2–4], an additional aspect, namely the splitting of a Landau band into a complicated system of subbands [5, 6] arises. Posing a real challenge for experimentalists, only recently some indications of such splitting were observed in magnetoresistance oscillations of small-period lateral superlattices [7].

The splitting of a Landau band into a number of subbands also leads to the redistribution of the quantum Hall (QH) current among them. While the total current in a band is conserved, and the QH conductance associated with each subband is still an integer (in units e^2h^{-1}), this integer need not equal unity [8, 9]. The detection of nontrivial, that is different from 0 or 1, QH

0953-8984/01/143365+15$30.00

conductances is of great experimental interest, however, the complexity of such a measurement (at least, in smooth periodic potentials) is even greater than that of the detection of subbands themselves. The reason for this lies in the fact that the subbands tend to arrange themselves into a hierarchical structure [5, 6] by forming clusters separated by large gaps, while inside each cluster smaller sub-clusters separated by smaller subgaps are formed. Having resolved the cluster structure at the coarsest level one would find that one cluster is carrying the total band's current while the others do not contribute at all. Thus, trying to access higher integers in the QH current distribution offers an immensely difficult task of resolving at least the second order sub-splittings. A recent experiment [10] considered the situation where the partial contributions of three subbands to the total QH current follow the pattern 1, -1, 1, so that the net conductance would show oscillations between 0 and 1. Due to the smallness of the minigaps the QH conductances did not fully attain the expected values, however, the indicative nonmonotonicity was clearly visible. In the present paper, we show that if the periodic potential is not smooth but rather composed of steep antidots, the distribution of band-widths among the subbands can be made very different thus increasing the feasibility of experimental access to the subbands carrying nontrivial QH currents. Moreover, we find that sufficiently steep potential profiles are not smoothed away by the screening charge of electrons.

Attempts to address the complicated topic of electron motion in a periodic potential and a competing magnetic field theoretically date back to the 1950's. The simplest descriptive model, known as Harper's equation [11], was derived in two limiting cases: (i) that of a weak perturbative periodic potential imposed upon otherwise flat Landau levels [12, 13], and (ii) that of a single tight-binding band subjected to a weak magnetic field [11, 12]. The efforts culminated in Hofstadter's calculation [6] of splitting and clustering of subbands into a complicated pattern depending on the ratio of the magnetic flux through a unit cell to the magnetic flux quantum. This treatment was based on the so-called Peierls substitution [14] and had a fairly limited range of validity [15], however it gave a qualitatively correct visualization of the phenomenon.

Later on, the technological advances renewed the theoretical interest in the field calling for a more realistic treatment. Harper's equation was generalized [16] to include interband coupling and thus properly accounted for predominant chaotic trajectories [17] in the near-classical regime. The electron–electron interaction was still not addressed. Its study was initiated [18] by introducing a self-consistency procedure using the Ferrari basis [19] into the band structure calculations. In this method one explicitly constructs translationally invariant states thus taking the crystal symmetry into account. In practice, however, the method turned out to be computationally demanding and provided answers only for a set of special (integer) magnetic fields and unusually low electron densities [18]. Thus, a new effort to address a dense set of (rational) magnetic fields and Coulomb repulsion between electrons was clearly needed.

In the present paper, we put forward a computational scheme capable of dealing with both integer and rational magnetic fluxes at the same level of complexity. We base this on the treatment of crystal symmetry in magnetic fields [20], and its application by Schellnhuber and co-workers [21, 22] to calculations of diamagnetic band structure in three-dimensional solids. In a previous publication [23] we treated the energy spectra of 2DES in the case of integer fluxes and smooth potentials.

After the original investigation by Thouless *et al* [8], the problem of the distribution of QH currents among subbands in a single band approximation was recently discussed by Chang and Niu [24] from the point of view of semiclassical electron dynamics. The changes induced by coupling between several Landau bands were addressed in [25]. In the present paper we extend the previous investigations by (i) showing that superlattices composed of steep antidots

provide a systematic way of increasing the widths of interesting (from the point of view of QH measurement) subgaps and (ii) including and discussing the role of the electron–electron interactions.

The paper has the following structure. In section 2 the model is formulated and in section 3 the symmetry-based analytical scheme is derived. In section 4 we discuss some limiting cases and carry out a calculation of the band structure of antidot superlattices paying particular attention to the appearance of an isolated cluster of subbands that splits off from a Landau band. Such subbands (we refer to them as 'levitating'), being considerably broad and isolated from the other ones by large gaps, increase our hopes that they (or even their internal structure) can be more easily resolved in an experiment and reveal some nontrivial QH numbers. We conclude with a summary in section 5, while some matters are dealt with in the appendices.

2. Model

We consider a 2D antidot superlattice and its reciprocal counterpart spanned by the respective vectors $\boldsymbol{R} = n_1\boldsymbol{a}_1 + n_2\boldsymbol{a}_2$ and $\boldsymbol{G} = g_1\boldsymbol{b}_1 + g_2\boldsymbol{b}_2$ with $n_{1(2)}, g_{1(2)} \in \mathcal{Z}$ and $\boldsymbol{a}_i \cdot \boldsymbol{b}_j = 2\pi\delta_{ij}$. While no special restrictions on the point symmetry are imposed, it is convenient to choose $\boldsymbol{a}_2 \parallel y$ so that $\boldsymbol{b}_1 \parallel x$. In a non-orthogonal lattice, $\boldsymbol{a}_1$ will also have a component along y, so we introduce the lattice 'skewness' parameter $s = a_{1y}/a_{2y}$ for this case. The independent-particle Hamiltonian of an electron moving in the crystal potential of such a lattice and a perpendicular magnetic field reads

$$H = \frac{1}{2m}\left(\boldsymbol{p} + \frac{e}{c}\boldsymbol{A}\right)^2 + \sum_{\boldsymbol{G}} v(\boldsymbol{G})\mathrm{e}^{\mathrm{i}\boldsymbol{G}\cdot\boldsymbol{r}}. \tag{1}$$

Here, the periodic potential is given in terms of its Fourier components $v(\boldsymbol{G})$ and the magnetic field is expressed via its symmetric-gauge vector potential $\boldsymbol{A}(\boldsymbol{r}) = \frac{1}{2}[\boldsymbol{B}\times\boldsymbol{r}]$. Our method can treat all so-called rational fields, i.e. such that the magnetic flux per unit cell equals a rational number of magnetic flux quanta $\Phi_0 = ch/e$:

$$\Phi/\Phi_0 = L/N \qquad L, N \in \mathcal{Z}. \tag{2}$$

Concentrating on the physics that is not crucially influenced by the electron spin, we neglect the exchange interaction and Zeeman splitting but do take the degeneracy due to spin into account.

The electrons are described in the effective-mass approximation using $m = 0.067\,m_0$ moving in a medium of dielectric constant $\kappa = 12.4$. We concentrate on short-period superlattices. In the calculation we set the lattice constant to $a = 1000$ Å; then a moderate magnetic field $B = 1.65$ T produces a commensurate flux equal to 4 flux quanta per unit cell. The Coulomb repulsion is included at the mean-field level. Thus, the periodic potential entering (1) is a sum of the 'external' antidot potential and the Hartree term

$$v(\boldsymbol{G}) = v^{\mathrm{ext}}(\boldsymbol{G}) + \frac{2\pi}{|\boldsymbol{G}|}\frac{\mathrm{e}^2}{\kappa}n_s(\boldsymbol{G})(1-\delta_{G,0}) \tag{3}$$

where $n_s(\boldsymbol{G})$ is the Fourier transformed electron density constructed from the eigenfunctions of the Hamiltonian in equation (1), and the Kronecker delta indicates that the $\boldsymbol{G} = 0$ contribution is cancelled by the positive background charge. Thus, the energy spectrum of Hamiltonian (1) has to be calculated self-consistently by convergent iterations together with equation (3).

In order to make use of the symmetry with respect to discrete translations in a uniform magnetic field we introduce the group of magnetotranslation operators. Their generator is

defined so as to commute with the kinetic momentum $\boldsymbol{p}_{\mathrm{kin}} = \boldsymbol{p} + \frac{e}{c}\boldsymbol{A}$, and in the symmetric gauge reads $\boldsymbol{p}_{\mathrm{gen}} = \boldsymbol{p} - \frac{e}{c}\boldsymbol{A}$. Therefore, we have

$$T_M(\boldsymbol{R})\psi(\boldsymbol{r}) = \exp\left[-\frac{\mathrm{i}}{\hbar}\boldsymbol{R}\cdot\left(\boldsymbol{p} - \frac{e}{c}\boldsymbol{A}\right)\right]\psi(\boldsymbol{r}) = \exp\left(\frac{\mathrm{i}e}{2\hbar c}\boldsymbol{r}\cdot[\boldsymbol{R}\times\boldsymbol{B}]\right)\psi(\boldsymbol{r}-\boldsymbol{R}). \quad (4)$$

The operators T_M appearing in equation (4) commute with the Hamiltonian (1) thus allowing for a classification of its eigenstates by their translational symmetry properties. Note, however, that a product of two magnetotranslations equals another member of the group only up to a phase

$$T_M(\boldsymbol{R}_1)T_M(\boldsymbol{R}_2) = T_M(\boldsymbol{R}_1+\boldsymbol{R}_2)\mathrm{e}^{-(\mathrm{i}e/2\hbar c)\boldsymbol{B}\cdot[\boldsymbol{R}_1\times\boldsymbol{R}_2]} \quad (5)$$

indicating that one deals here with a ray group [26] rather than a conventional vector group. Nevertheless, the conventional framework of group-theoretical treatment remains applicable [20].

3. Theory

Having spelled out all the definitions in full in the preceding section 2, we now switch to natural dimensionless units. We use the cyclotron frequency and the magnetic length

$$\omega_c = \frac{eB}{mc} \qquad l_c = \sqrt{\frac{\hbar c}{eB}} \quad (6)$$

as the defining quantities, and from now on measure all lengths in l_c, momenta in $\hbar l_c^{-1}$, and energies in $\hbar\omega_c$. The rationality condition (2) is cast into a relation for the unit-cell area

$$\Omega = a_{1x}a_{2y} = 2\pi L/N \quad (7)$$

to be extensively used in algebraic manipulations hereafter.

Further, we perform a canonical coordinate transformation [22] to a new set of variables ξ and η

$$\begin{aligned} \xi &= p_y + x/2 \qquad & p_\xi &= p_x - y/2 \\ \eta &= -p_y + x/2 \qquad & p_\eta &= p_x + y/2 \end{aligned} \quad (8)$$

which maps the kinetic-energy part of the Hamiltonian (denoted H_0) onto that of a harmonic oscillator in ξ

$$H_0 = \frac{1}{2}\left(p_\xi^2 + \xi^2\right). \quad (9)$$

Moreover, the translations (4) are now found to act only on the η coordinate

$$T_M(\boldsymbol{R}) = \exp(-\mathrm{i}R_x p_\eta + \mathrm{i}R_y\eta). \quad (10)$$

Thus, the complexity has been isolated into the periodic potential term which has become a function of both the new coordinates and momenta. Its Fourier components behave like magnetic translation operators

$$\begin{aligned} H_1 &= \sum_{\boldsymbol{G}} v(\boldsymbol{G})\hat{X}(\boldsymbol{G}|\xi)\hat{Y}(\boldsymbol{G}|\eta) \\ \hat{X}(\boldsymbol{G}|\xi) &= \exp(\mathrm{i}G_x\xi - \mathrm{i}G_y p_\xi) \\ \hat{Y}(\boldsymbol{G}|\eta) &= \exp(\mathrm{i}G_x\eta + \mathrm{i}G_y p_\eta) \end{aligned} \quad (11)$$

and will mix the ξ and η degrees of freedom.

The transformation of states between (x, y) and (ξ, η) representations is given by

$$\langle xy|\psi\rangle = \int_{-\infty}^{\infty} \mathrm{d}\xi \int_{-\infty}^{\infty} \mathrm{d}\eta \, \langle xy|\xi\eta\rangle\langle\xi\eta|\psi\rangle \tag{12}$$

with the kernel $\langle xy|\xi\eta\rangle$ obtained by solving the eigenvalue equations for ξ and η

$$\left(\frac{x}{2} - \mathrm{i}\frac{\partial}{\partial y} - \xi\right)\langle xy|\xi\eta\rangle = 0$$
$$\left(\frac{x}{2} + \mathrm{i}\frac{\partial}{\partial y} - \eta\right)\langle xy|\xi\eta\rangle = 0 \tag{13}$$

with the result

$$\langle xy|\xi\eta\rangle = \frac{1}{\sqrt{2\pi}}\mathrm{e}^{\mathrm{i}y(\xi-\eta)/2}\delta(x - \xi - \eta). \tag{14}$$

3.1. Symmetry adapted basis

In order to take full advantage of the symmetry properties of the system, the next step towards a solution is the decomposition of the functional space $\mathcal{F}(\xi, \eta)$ of all functions of ξ and η into invariant subspaces of the symmetry group. Since the different subspaces are not coupled by the Hamiltonian, the effort needed to diagonalize it is reduced. Moreover, thanks to the canonical transformation the magnetotranslations now act only on the η degree of freedom, so the task narrows to a construction of a symmetry-adapted basis that spans $\mathcal{F}(\eta)$. As we will see, the dimensionality of the invariant subspaces equals L, therefore the ansatz for the states will involve a linear combination of L η-dependent functions multiplied by a suitable expansion of the ξ-dependent part.

The construction of the symmetry-adapted basis for the η degree of freedom proceeds by employing the projection-operators technique. We use the irreducible representations of the magnetotranslation group given in [20]. They are labelled by the magnetic crystal momentum vector $\boldsymbol{q} = q_1\boldsymbol{b}_1 + q_2\boldsymbol{b}_2$ and relate to the 'central' ($\boldsymbol{q} = 0$) one as

$$D^{\boldsymbol{q}}(\boldsymbol{R}) = \mathrm{e}^{-\mathrm{i}\boldsymbol{q}\cdot\boldsymbol{R}}D^0(\boldsymbol{R}) = \mathrm{e}^{-2\pi\mathrm{i}(n_1q_1+n_2q_2)}D^0(\boldsymbol{R}). \tag{15}$$

The $N \times N$ matrix D^0 for any translation vector $\boldsymbol{R}$ is generated from those corresponding to the primitive lattice vectors [20][1]

$$D^0_{jk}(\boldsymbol{a}_1) = \delta_{jk}\mathrm{e}^{2\pi\mathrm{i}(j-1)L/N} \quad D^0_{jk}(\boldsymbol{a}_2) = \delta^{\bmod N}_{j,k-1} \tag{16}$$

and the ray-group multiplication law (5) yielding

$$D^0_{jk}(\boldsymbol{R}) = \delta^{\bmod N}_{j,k-n_2} \exp\left\{\mathrm{i}\pi\frac{L}{N}n_1[n_2 + 2(j-1)]\right\}. \tag{17}$$

Note that increasing any of q_1 or q_2 by $1/N$ produces an equivalent representation. Thus the values of $\boldsymbol{q}$ have to be restricted to a single magnetic Brillouin zone (MBZ) which we choose as $0 \leqslant q_1, q_2 < 1/N$. The rank of the matrices implies the existence of N partner functions (indexed by $t = 1, \ldots, N$) transforming according to different rows of the same irreducible representation D^q. However, in the subsequent analysis we concentrate only on one ($t = 1$) of the partners for the others can be easily obtained from it by means of a translation parallel to $\boldsymbol{a}_2$. This and other transformation properties of the states are discussed in appendix A.

[1] From here on we use the notation $\delta^{\bmod p}_{ij}$ to denote a 'modulo Kronecker delta' which equals 1 if i and j are equal or differ by a multiple of p, and vanishes otherwise.

In order to construct the principal partner function we introduce the projection operator projecting onto the first row of the $\boldsymbol{q}$th representation

$$P^{q}_{11} = \sum_{\boldsymbol{R}} [D^{q}_{11}(\boldsymbol{R})]^{*} T_{M}(\boldsymbol{R}). \tag{18}$$

After a number of straightforward algebraic steps (see appendix B for some details and comments) we arrive at the following expressions for the normalized basis functions labelled by a new subband index ($l = 0, 1, \ldots, L-1$) introduced to account for the presence of L linearly independent basis functions of the same symmetry

$$\varphi_{l}(\boldsymbol{q}|\eta) = \sqrt{\frac{2\pi}{a_{2y}}} \sum_{m=-\infty}^{\infty} \exp\left[2\pi \mathrm{i} m\,(q_1 - s q_2) + \mathrm{i}\pi s \frac{m^2 L + 2ml}{N}\right] \times \delta\left(\eta + N q_2 \frac{a_{1x}}{L} - a_{1x}\frac{l + Lm}{L}\right). \tag{19}$$

These functions together with the other partner functions constitute a complete orthonormal set in $\mathcal{F}(\eta)$. By construction, the Hamiltonian is diagonal with respect to the quantum numbers q_1, q_2 and t but can mix different subbands l.

3.2. Eigenvalue problem

Turning to the ξ-dependent part of the wave-function, we see that it can be expanded in any suitable basis independent of the symmetry. Working in the strong magnetic field limit, the harmonic oscillator eigenfunctions $\chi_n(\xi)$ are an appropriate choice. In this case the kinetic energy H_0 is immediately diagonal and the task is to diagonalize H_1. In simple terms, this means that one deals with perturbed Landau levels.

Specializing this approach, we formulate the following ansatz for the states

$$\psi(\boldsymbol{q}|\xi, \eta) = \sum_{n=0}^{\infty} \chi_n(\xi) \sum_{l=0}^{L-1} a_{nl} \varphi_l(\boldsymbol{q}|\eta) \tag{20}$$

which allows for mixing of different Landau levels and subbands. Upon insertion into the Hamiltonian, one sees that the effect of the operator $\hat{Y}(\boldsymbol{G}|\eta)$ can be expressed as

$$\hat{Y}(\boldsymbol{G}|\eta)\varphi_{l'}(\boldsymbol{q}|\eta) = \sum_{l=0}^{L-1} A_{ll'}(\boldsymbol{q}; \boldsymbol{G})\varphi_{l}(\boldsymbol{q}|\eta) \tag{21}$$

where $A_{ll'}$ is a phase factor whose calculation is straightforward and yields

$$A_{ll'}(\boldsymbol{q}; \boldsymbol{G}) = \exp\left(\mathrm{i}\pi g_1 g_2 \frac{N}{L}\right) \exp\left(2\pi \mathrm{i} g_1 \frac{l}{L}\right) \exp\left[2\pi \mathrm{i} \frac{N}{L}(q_1 g_2 - q_2 g_1)\right] \times \exp\left[2\pi \mathrm{i}\,(q_1 - s q_2)\,\frac{l - l'}{L}\right] \exp\left(\mathrm{i}\pi s \frac{l^2 - l'^2}{NL}\right) \delta^{\bmod L}_{l', l + N g_2}. \tag{22}$$

Similarly, the effect of $\hat{X}(\boldsymbol{G}|\xi)$ on a harmonic oscillator function can be written

$$\hat{X}(\boldsymbol{G}|\xi)\chi_{n'}(\xi) = \sum_{n=0}^{\infty} B_{nn'}(\boldsymbol{G})\chi_{n}(\xi) \tag{23}$$

thus mixing Landau levels. Using the defining equation (11) we express the ξ-dependent matrix element (23) as

$$B_{nn'}(\boldsymbol{G}) = \mathrm{e}^{-\mathrm{i}G_xG_y/2}\int_{-\infty}^{\infty}\chi_n(\xi)\chi_{n'}(\xi - G_y)\mathrm{e}^{\mathrm{i}G_x\xi}\mathrm{d}\xi$$
$$= \sqrt{\frac{2^{n'}n'!}{2^n n!}}\mathrm{e}^{-(G_x^2+G_y^2)/4}(G_y + \mathrm{i}G_x)^{n-n'}L_n^{n-n'}\left(\frac{G_x^2+G_y^2}{2}\right) = B^*_{n'n}(-\boldsymbol{G}) \qquad (24)$$

for $n \geqslant n'$.

The result of the above manipulations is the following eigenvalue problem

$$\sum_{n'=0}^{\infty}\sum_{l'=0}^{L-1}\mathcal{M}_{nl;n'l'}a_{n'l'} = \epsilon a_{nl}$$
$$\mathcal{M}_{nl;n'l'} = \delta_{nn'}\delta_{ll'}\left(n+\frac{1}{2}\right) + \sum_{\boldsymbol{G}} v(\boldsymbol{G})A_{ll'}(\boldsymbol{q};\boldsymbol{G})B_{nn'}(\boldsymbol{G}) \qquad (25)$$

whose solutions specify the single particle states and energies. Transforming the symmetry-adapted basis functions $\psi_{nl}(\boldsymbol{q}|\xi\eta) = \chi_n(\xi)\varphi_l(\boldsymbol{q}|\eta)$ into the x and y coordinates according to (14) and we obtain

$$\psi_{nl}(\boldsymbol{q}|xy) = \frac{1}{\sqrt{a_{2y}}}\mathrm{e}^{\mathrm{i}xy/2}\sum_{m=-\infty}^{\infty}\mathrm{e}^{2\pi\mathrm{i}m(q_1-sq_2)}\mathrm{e}^{\mathrm{i}\pi s(m^2+2ml)/N}\mathrm{e}^{-\mathrm{i}\kappa_{lm}y}\chi_n(x-\kappa_{lm})$$
$$\kappa_{lm} = a_{1x}\left(-\frac{Nq_2}{L} + \frac{l+mL}{L}\right). \qquad (26)$$

The chosen normalization

$$\int_{-\infty}^{\infty}\mathrm{d}x\int_{-\infty}^{\infty}\mathrm{d}y\,\psi^*_{n'l'}(\boldsymbol{q}'|xy)\psi_{nl}(\boldsymbol{q}|xy) = \delta(q_1-q_1')\delta(q_2-q_2')\delta_{nn'}\delta_{ll'} \qquad (27)$$

implies that the states are normalized to N over N adjacent cells along $\boldsymbol{a}_2$.

We express the eigenstates in real space as

$$\psi^{(\nu)}(\boldsymbol{q}|xy) = \sum_{n=0}^{\infty}\sum_{l=0}^{L-1}a_{nl}^{(\nu)}\psi_{ln}(\boldsymbol{q}|xy) \qquad (28)$$

where ν numbers the different solutions of equation (25). The Fourier components of electron charge density are obtained by Fourier transforming

$$n_s(\boldsymbol{r}) = 2\sum_{\boldsymbol{q},\nu,t}|\psi^{(\nu)}(\boldsymbol{q},t|\boldsymbol{r})|^2 f\,[\epsilon_\nu(\boldsymbol{q}) - \mu] \qquad (29)$$

where 2 is for spin, $f(\epsilon - \mu)$ denotes the Fermi distribution function and μ is the chemical potential determined by equating the integral of (29) over a unit cell to the average number of electrons per cell. In order to improve the numerical stability, we perform the calculations at several small but finite values of the temperature and then extrapolate to $T = 0$ [27].

It has been shown that the quantized value of QH current carried by a given subband is determined by the total vorticity of the wave-function in MBZ [8,28]. Therefore, the knowledge of energy levels and eigenstates will also specify the QH conductances obtained whenever the chemical potential lies in a gap thus separating the completely filled subbands from the empty ones. A practical way of computing the QH integers σ_H in a gap is given by the thermodynamic Středa formula [9]

$$\frac{e^2}{h}\sigma_H = ec\left[\frac{\partial N(E)}{\partial B}\right] \qquad \sigma_H \in \mathcal{Z} \qquad (30)$$

which expresses the conductance in terms of the dependence of the number of electronic states below the gap on the magnetic field strength. Being able to handle a dense set of rational fields, we obtain σ_H directly from the band-structure calculations at two sufficiently close values of magnetic flux that share the gap.

4. Results

Let us now turn to the results obtained applying the above formalism to antidot superlattices. We begin our presentation by contrasting the essential features of the energy spectra of non-interacting electrons for two distinct choices of the periodic potential: (i) smooth potentials described by a few lowest Fourier components and (ii) potentials created by very narrow and steep antidots whose Fourier spectrum includes many high-$\boldsymbol{G}$ components. In the extreme limits of the two cases we deal with a cosine-like modulation and a lattice of δ-functions, respectively, and obtain some analytical results. In the second case, we record the property of the energy spectrum to contain split-off levitating subbands and proceed to consider realistic antidots of finite radius and include the effects of electron–electron interaction.

4.1. Weak cosine modulation

We now concentrate on the lattices of perfect square symmetry and describe the potential modulation by setting the four lowest Fourier components to equal strength $v(0,\pm1) = v(\pm1,0) \equiv v$. When the potential is also weak, the different Landau levels are not coupled ($B_{nn'} \propto \delta_{nn'}$) and all four non-vanishing coefficients $B_{nn}(\boldsymbol{G})$ are equal and evaluate to

$$b_n \equiv B_{nn}(0,\pm1) = B_{nn}(\pm1,0) = \mathrm{e}^{-\pi N/(2L)} L_n\left(\frac{\pi N}{L}\right). \tag{31}$$

Consequently, b_n can be moved outside the sum over $\boldsymbol{G}$ in the potential-energy term of equation (25) as a prefactor, and thus it will influence only the overall band widths. The internal subband structure within each band will be given by the rest of the summation which we carry out explicitly. For the sake of convenience, we redefine the phases of the wave functions according to $\varphi_l(\boldsymbol{q}) \to \varphi_l(\boldsymbol{q})\exp(2\pi i q_1 l/L)$. Then the potential energy term reduces to $v b_n \delta_{nn'} \Xi_{ll'}$, the matrix Ξ containing the following non-zero matrix elements

$$\begin{aligned} \Xi_{ll} &= 2\cos\left[\frac{2\pi}{L}(l - Nq_2)\right] \\ \Xi_{lm} &= \Xi^*_{ml} = \exp\left(2\pi \mathrm{i}\frac{N}{L}q_1\right)\delta^{\bmod L}_{l+N,m}. \end{aligned} \tag{32}$$

Renumbering the rows and columns of this matrix according to $l = N\lambda \bmod L$ it can be cast into the form[2]

$$\begin{aligned} \Xi_{\lambda\lambda} &= 2\cos\left[2\pi\frac{N}{L}(\lambda - q_2)\right] \\ \Xi_{\lambda\mu} &= \Xi^*_{\mu\lambda} = \exp\left(2\pi \mathrm{i}\frac{N}{L}q_1\right)\delta^{\bmod L}_{\lambda+1,\mu} \end{aligned} \tag{33}$$

allowing for the following interpretation. As depicted in figure 1, one deals with a 1D chain of lattice sites whose energies are modulated by a cosine function of period L/N. Neighbouring sites are coupled by hopping matrix elements of unit absolute magnitude and incorporating a phase $\Delta = 2\pi N q_1/L$.

[2] Since N and L are mutual primes, such a renumbering is always possible. Note also that in this subsection we number the matrix indices from 0 to $L-1$.

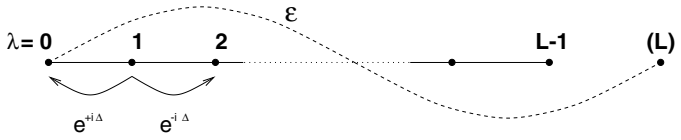

Figure 1. A 1D chain of L lattice sites with periodic boundary conditions. The site energies are modulated according to the law $\varepsilon_\lambda = 2\cos[2\pi N(\lambda - q_2)/L]$ so that one has an integer number (N) of full periods per L sites. The hopping matrix elements include a phase $\Delta = 2\pi N q_1/L$.

The matrix Ξ embodies the simplest model describing commensurability-related phenomena equivalently to the Harper's equation. In the present case we encounter the commensurability between the unit lattice site spacing and L/N site energy modulation period which leads to the splitting of each Landau band into L subbands. This observation completes the demonstration of how our model reduces to previously known simple models [6]. For the sake of reference, we also need to quote some results. Thus, in figure 2 we show the relative widths of the subbands together with the QH currents carried by each of them for a few flux values close to $L/N = 3$. The important point to note is that the physical requirement for the bands to evolve continuously as a function of magnetic field leads to the clustering of the subbands into closely packed groups denoted by 'A', 'B' and 'C' whose net QH conductances equal 0, 1 and 0, respectively. When the commensurate flux deviates from the value $L/N = 3/1$, the three clusters develop a fine structure of subbands carrying QH currents different from 0 or 1. We note that these subbands and subgaps separating them are narrow and thus difficult to resolve. However, the subband structure can be quite different in a periodic lattice whose potential is steep and thus posesses a broad Fourier spectrum.

4.2. δ-function antidot lattice

We start by considering integer fluxes L (i.e. $N = 1$), while the discussion of the general case of rational fluxes follows later. The periodic lattice is composed of antidots modelled by δ-functions, thus

$$v(\boldsymbol{r}) = v_0\Omega\sum_{\boldsymbol{R}}\delta(\boldsymbol{r}-\boldsymbol{R}) \qquad v(\boldsymbol{G}) \equiv v_0 \tag{34}$$

in the real and reciprocal space, respectively. Here v_0 is the strength of an antidot and Ω is the unit-cell area. Calculating the matrix elements of potential (34) in the symmetry-adapted basis (26) we find

$$\int_{-\infty}^{\infty}\mathrm{d}x\int_{-\infty}^{\infty}\mathrm{d}y\;\psi^*_{nl}(\boldsymbol{q}|\boldsymbol{r})v(\boldsymbol{r})\psi_{n'l'}(\boldsymbol{q}'|\boldsymbol{r}) = v_0\Omega\delta(q_1-q_1')\delta(q_2-q_2')\psi^*_{nl}(\boldsymbol{q}|0)\psi_{n'l'}(\boldsymbol{q}|0). \tag{35}$$

Thus we see that at each point in MBZ the matrix of the potential energy factorizes into an outer product of a vector with itself. Such a matrix has only one non-zero eigenvalue.

In the limit of weak potentials v_0 the coupling between different Landau levels can be neglected. Then we find the energies of the states with respect to the common energy $n + 1/2$ in the nth level[3] by diagonalizing just the $L \times L$ potential energy matrix $v_{ll'} = v_0\Omega\,\psi^*_{nl}(\boldsymbol{q}|0)\psi_{nl'}(\boldsymbol{q}|0)$. In view of its special structure all but one of its eigenvalues equal zero and the only nonvanishing one is obtained as the trace

$$\varepsilon_n(\boldsymbol{q}) = v_0\Omega\sum_{l=0}^{L-1}|\psi_{nl}(\boldsymbol{q}|0)|^2. \tag{36}$$

[3] We number Landau levels starting with zero for the lowest one.

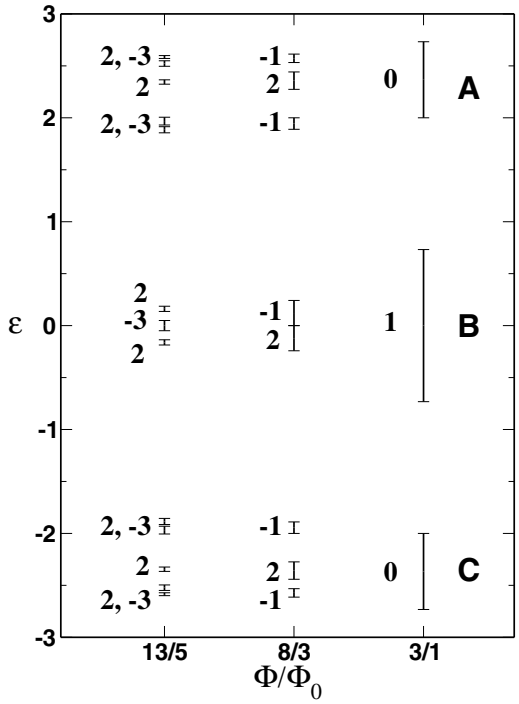

Figure 2. The structure of the energy spectrum and distribution of quantum Hall curents among the subbands for several magnetic flux values close to $L/N = 3$. The continuity of the subbands leads to the 'hiding' of nontrivial QH integers in deep levels of the recursive subband structure.

Thus we conclude that in the perturbative regime the lattice of δ-antidots will split off exactly one subband from each Landau band containing L subbands in total. This in turn implies that the degenerate subband wave-functions rearrange themselves in such a way that $L-1$ of them have their zeros at the locations of antidots so that they are not affected by the zero-range antidot potential. Therefore, even beyond the perturbative regime one will still observe only one split-off subband, however, its energy will not scale linearly with the potential strength but rather level off. We display both the linear dispersion in the perturbative regime and the cross-over to the 'saturation' region of the band energies in the panel (a) of figure 3 for a magnetic flux $L = 4$.

Another interesting feature shown in figure 3(a) is that the lower edge of the levitating subband in the third ($n = 3$) Landau band stays pinned exactly at the value $\varepsilon = 3.5$ regardless of the potential strength. This is a consequence of the fact that in the present case at the centre of MBZ (which corresponds to the band minimum) *all four* subband functions have their zeros at the exact locations of the antidots and thus are not affected by the potential at all. On the contrary, at the corner of MBZ ($q_1 = q_2 = 1/2$, top of the band) all four unperturbed functions place their maxima at the locations of the antidots. Therefore, the resulting energy (36) is large, and the band is broad.

However, panel (b) displays the behaviour of the same bands when the potential strength and the magnetic flux penetrating a unit cell are kept fixed at the respective values $v_0 = 0.15$ and $L = 4$, but the shape of the lattice is varied by continuously distorting it into a rectangular (rather than square) one. We observe that at some given ratio of the two lattice constants the width of the third band shrinks down to zero. On the contrary, the width of the levitating

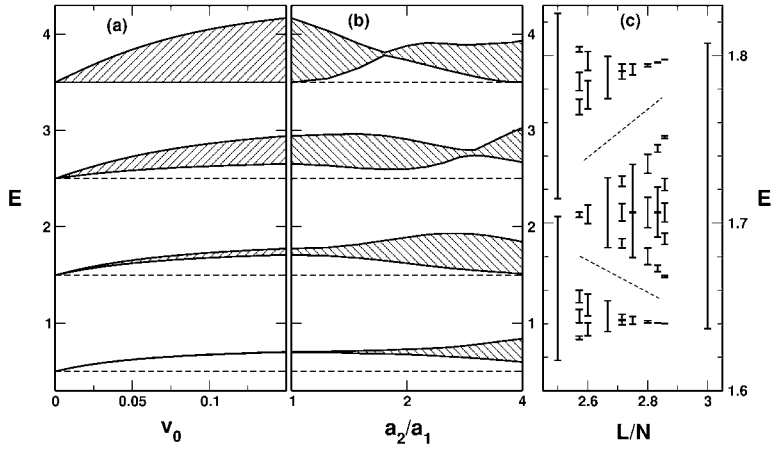

Figure 3. The structure of the energy spectrum in a δ-antidot lattice. Panel (a) shows the evolution of the split-off levitating subbands at a fixed integer magnetic flux $\Phi = 4\Phi_0$ as a function of potential strength. The energies are measured in units $\hbar\omega_c = 2.86$ meV. The remaining 3 subbands in each Landau band have zero widths and are positioned at the unperturbed energies $n + 1/2$ denoted by dashed lines. In (b) we display the band-widths as a function of the ratio of two lattice constants (logarithmic scale) at fixed values of $v_0 = 0.15$ and $L = 4$. (c) shows the dispersion against the magnetic field of the levitating subband belonging to the $n = 1$ Landau level for a fixed value of the potential $v_0 = 0.125$ in a square lattice. We look at the vicinity of $L/N = 3/1$ and correspondingly measure energies in units $\hbar\omega_c = 2.14$ meV.

subband originating from the lowest Landau level increases quite substantially starting from what was a very narrow band in a square lattice. In conclusion, the subband wave-functions exibit a certain rigidity and thus the effect of a periodic δ-function lattice on the energy spectrum depends on the relative distribution of the lattice sites, on one hand, and maxima and nodes of the states, on the other.

The levitating subbands contain a magnetic field independent number of states and therefore carry no net QH current. However, for rational fluxes ($N \neq 1$) each of these bands splits into N smaller subbands. Being able to resolve such splittings inside a levitating band one would detect some interesting QH currents. In figure 3(c), we show the fine structure of a levitating subband in the vicinity of commensurate flux $L/N = 3$. The three most conspicuous clusters separated by large gaps (denoted by dashed lines) carry QH currents equal to -1, 2, -1.

Comparing the discussed structure of the spectrum to that found in the limit of smooth potentials we can describe it as the magnification of the energy scale of the topmost cluster of subbands denoted by 'A' in figure 2 while the widths of clusters 'B' and 'C' shrink down to zero. This redistribution of band-widths can be used as a way to *systematically* increase the widths of certain subbands and gaps in the 'butterfly'-like bandstructure when trying to detect them experimentally, in particular, in a QH measurement. We suggest that broad levitating subbands could be most easily detected in moderate ($L/N \approx 3-6$) magnetic fields. In weaker fields, the electronic states are poorly localized and thus they are averaging the potential landscape over a large area of a unit cell. Therefore, even very narow antidots will fail to differentiate between various degenerate subband states in a Landau level. On the other hand, in stronger magnetic fields the states in a levitating subband become too strongly localized and have vanishingly small overlaps with their neighbours in adjacent cells which results in very small band-widths. Moreover, as we discussed above, the widths and positions of the levitating subbands may be very sensitive to the geometry of the lattice.

4.3. Realistic antidot superlattices

With the discussion of limiting cases in the background, we proceed to the consideration of superlattices of finite-radius antidots and also include the electron–electron interaction. We set the electron density to $n_s = 10^{11}$ cm^{-2}. The lattice is chosen to be of perfect square symmetry, and the antidots are modelled by gaussians of effective radius b. Thus, in the real and reciprocal space, respectively,

$$v(\boldsymbol{r}) = \sum_{\boldsymbol{R}} v_0 \, \mathrm{e}^{-(r-\boldsymbol{R})^2/b^2} \qquad v(\boldsymbol{G}) = v_0 \alpha \mathrm{e}^{-\alpha \pi g^2} \tag{37}$$

here $g = (g_1^2 + g_2^2)^{1/2}$ and $\alpha = \pi b^2/a^2$ denotes the fraction of a cell area occupied by an antidot.

The panels (a) and (b) of figure 4 show the subband structure in the first ($n = 1$) Landau band for the magnetic flux $L/N = 3$. We plot the allowed energy values in the three resulting subbands as a function of the effective electron–electron interaction strength λ which is 'turned on' from 0 (free electrons) to 1 (actual value). The two panels compare the spectra obtained for two different sizes of antidots: $\alpha = 0.1$ and 0.2 in the panels (a) and (b), respectively.

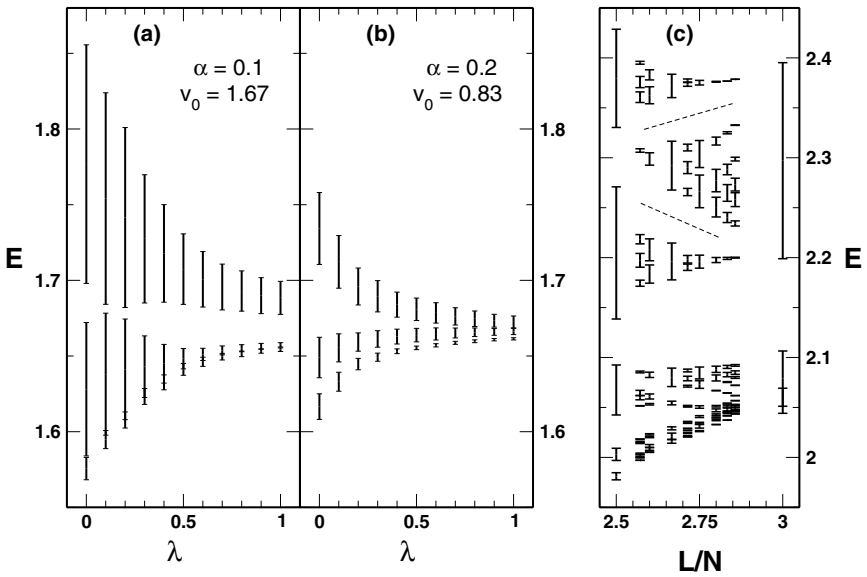

Figure 4. The energy spectra of interacting electrons in units $\hbar\omega_c = 2.14$ meV. The panels (a) and (b) show the behaviour of the subbands in the first Landau band as a function of effective interelectron interaction strength λ for two different choices of periodic potential (see parameter values in the figure). The panel (c) shows the subband structure versus magnetic flux for fully interacting electrons and $\alpha = 0.1$, $v_0 = 6.67$.

We see that the bands become narrower as the interaction strength increases. The reason for this lies in the fact that the band-widths are set by a competition between the band-narrowing effect due to the magnetic field and the broadening of the bands by the periodic potential. The electronic screening effectivelly reduces the strength of the periodic potential and consequently leads to narrower bands. The importance of the screening can be judged upon from the fact that the band-widths change ≈ 4 times.

However, in a lattice composed of narrow antidots ($\alpha \leqslant 0.1$) the strong screening effects fail to introduce qualitative changes into the structure of the energy spectrum since the Coulomb

potential in reciprocal space behaves as $\propto |\boldsymbol{G}|^{-1}$ and becomes inefficient at high $\boldsymbol{G}$'s. Thus, in figure 4(a) we see that even in the presence of electron–electron interaction the nature of the spectrum retains features characteristic of a narrow-antidot lattice. At $\lambda \approx 0.15$ we find a closing and reopening of the gap separating the levitating subband from the other two. However, it does not lead to redistribution of QH currents; the net current in the topmost band always equals 0. In panel (c), we plot the energy bands versus the commensurate magnetic flux for the interacting electrons ($\lambda = 1$). Here the value of v_0 is four times larger than that in panel (a) in order to maintain the overall width of the bands. As in figure 3, the three most conspicuous clusters of subbands (delimited by dashed lines) within the levitating band carry QH currents equal to -1, 2, -1 and are still separated by sufficiently broad gaps.

When the size of the antidots is increased to $\alpha = 0.2$ (panel (b)) the electronic screening becomes capable of transforming the steep bare periodic potential into a rather smooth self-consistent potential. Thus, we see that at the effective interaction around $\lambda \approx 0.3$ the nature of the subband structure cross-over to that characteristic of smooth potentials, i.e. the wide gap separating a levitating subband disappears.

The inclusion of exchange and correlation effects beyond the mean-field level would introduce certain *quantitative* modifications into the details of the self-consistent potential and the exact positions of the calculated bands, however, the essential conclusions regarding the nature of the energy spectrum and its stability with respect to strong electron–electron interactions follow from the inefficiency of screening of high Fourier components of the external potential and would remain unaltered.

5. Summary

In summary, we developed a theory to describe electrons moving in competing periodic potentials and magnetic fields which enabled us to treat interacting electrons at a dense set of magnetic field values. Considering the electron spectra in superlattices composed of steep antidots we identified a cluster of sufficiently broad and well isolated subbands. Such subbands can be more easily resolved in a measurement, moreover, their internal structure may reveal a rich spectrum of QH integers.

Appendix A. Symmetry properties of the states

The transformation properties of the states with respect to translations are derived by commuting the magnetic-translation operators (4) and a general projection operator

$$P^{\boldsymbol{q}}_{jk} = \sum_{\boldsymbol{R}} [D^0_{jk}(\boldsymbol{R}) \mathrm{e}^{-\mathrm{i}\boldsymbol{q}\cdot\boldsymbol{R}}]^* T_M(\boldsymbol{R}) \tag{A.1}$$

which projects out the component belonging to the k-th row of the representation $\boldsymbol{q}$ and then generates the partner belonging to the j-th row. After some straightforward algebra we obtain

$$\begin{aligned} T_M(-\boldsymbol{a}_1) P^{\boldsymbol{q}}_{jk} &= \mathrm{e}^{2\pi\mathrm{i}[q_1 - (L/N)(j-1)]} P^{\boldsymbol{q}}_{jk} \\ T_M(-\boldsymbol{a}_2) P^{\boldsymbol{q}}_{jk} &= \mathrm{e}^{2\pi\mathrm{i}q_2} P^{\boldsymbol{q}}_{j+1,k}. \end{aligned} \tag{A.2}$$

The first line in equation (A.2) defines the equivalent of the usual Bloch condition, while the second one equips us with a rule for generation of all partner functions from the first one

$$\psi_j(\boldsymbol{q}) = \mathrm{e}^{-2\pi\mathrm{i}q_2(j-1)} T_M[-(j-1)\boldsymbol{a}_2]\psi_1(\boldsymbol{q}). \tag{A.3}$$

Joining N adjacent cells along the $\boldsymbol{a}_2$ direction one constructs a supercell enclosing an *integer* flux and recovers a Bloch-like relation

$$T_M(N\boldsymbol{a}_2)\psi_j(\boldsymbol{q}) = \mathrm{e}^{-2\pi\mathrm{i}Nq_2}\psi_j(\boldsymbol{q}). \tag{A.4}$$

Appendix B. On the projection operators

We start by inserting the expression of irreducible representation (17) and the magnetotranslation operator (10) into the definition of the projection operator (18). In the resulting sum over lattice sites, the summations over the indices n_1 and n_2 decouple. The latter one can be carried out explicitly thus transforming a sum of exponentials into a series of δ-functions. The answer reads

$$P_{11}^{q} = \frac{a_{1x}}{L} \sum_{m=-\infty}^{\infty} \delta\left[\eta + (Nq_2 - m)\frac{a_{1x}}{L}\right] \sum_{n=-\infty}^{\infty} \mathrm{e}^{2\pi \mathrm{i} n q_1} \mathrm{e}^{-\mathrm{i} a_{1x} a_{1y} n^2/2} \mathrm{e}^{\mathrm{i} a_{1y} n \eta} T_\eta(n a_{1x}). \tag{B.1}$$

Consider first the case $L = 1$. Acting on a given seed function the translation operator T_η will produce its shifted replicas of period a_{1x} which will be subsequently filtered through a series of δ-functions of the same spacing. Thus, in order to be able to project out nonvanishing components for any subspace it suffices to choose a seed function that is nonzero (we set it equal to a constant) only in an interval of length a_{1x}. Consequently, the final expression for the states (19) contains just a single sum and not double series.

In the case $L \neq 1$ the spacing between δ-functions in (B.1) becomes L times finer and leads to the appearance of L distinct basis functions of the same symmetry.

Our procedure of constructing the symmetry-adapted basis bears some resemblance to that due to Ferrari [19]. The 'double series' in Ferrari's equation (45) is the equivalent of our projection operator. However, the corresponding expression for the states given in equation (46) of [19] still involves a double sum. Moreover, our approach based on group theory handles the cases $L \neq 1$, $N \neq 1$ in a uniform way without any need for introducion of a finer paving inside a lattice cell or explicit construction of supercells.

Acknowledgments

We acknowledge valuable discussions with Professor Algirdas Matulis and Dr. Carl-Olof Almbladh. One of us (PJ) was supported by the Swedish Natural Science Research Council (NFR).

References

[1] Weiss D, von Klitzing K, Ploog K and Weimann G 1989 *Europhys. Lett.* **8** 179
Gerhardts R R, Weiss D and von Klitzing K 1989 *Phys. Rev. Lett.* **62** 1173
Winkler R W, Kotthaus J P and Ploog K 1989 *Phys. Rev. Lett.* **62** 1177
[2] Weiss D, von Klitzing K, Ploog K and Weimann G 1990 *Surf. Sci.* **229** 88
[3] Gerhardts R R, Weiss D and Wulf U 1991 *Phys. Rev.* B **43** 5192
[4] Pfannkuche D and Gerhardts R R 1992 *Phys. Rev.* B **46** 12 606
[5] Azbel M Ya 1964 *Zh. Eksp. Teor. Fiz.* **46** 929 (Eng. Transl. 1964 *Sov. Phys.-JETP* **19** 634)
[6] Hofstadter D R 1976 *Phys. Rev.* B **14** 2239
[7] Schlösser T, Ensslin K, Kotthaus J P and Holland M 1996 *Semicond. Sci. Technol.* **11** 1582
[8] Thouless D J, Kohmoto M, Nightingale M P and den Nijs M 1982 *Phys. Rev. Lett.* **49** 405
Kohmoto M 1985 *Ann. Phys.* (NY) **160** 343
[9] Středa P 1982 *J. Phys. C: Solid State Phys.* **15** L717
Středa P 1982 *J. Phys. C: Solid State Phys.* **15** L1299
[10] Albrecht C, Smet J H, von Klitzing K, Weiss D, Umansky V and Schweizer H 2001 *Phys. Rev. Lett.* **86** 147
[11] Harper P G 1955 *Proc. Phys. Soc.* A (London) **68** 874
[12] Langbein D 1969 *Phys. Rev.* **180** 633
[13] Rauh A 1975 *Phys. Status Solidi* B **69** K9
[14] Peierls R E 1933 *Z. Phys.* **80** 763
[15] Alexandrov A S and Capellmann H 1991 *Phys. Rev. Lett.* **66** 365

[16] Petschel G and Geisel T 1993 *Phys. Rev. Lett.* **71** 239
[17] Weiss D, Roukes M L, Menschig A, Grambow P, von Klitzing K and Weimann G 1991 *Phys. Rev. Lett.* **66** 2790
Fleischmann R, Geisel T and Ketzmerick R 1992 *Phys. Rev. Lett.* **68** 1367
[18] Gudmundsson V and Gerhardts R R 1995 *Phys. Rev.* B **52** 16 744
Gudmundsson V 1998 *Phys. Rev.* B **57** 3989
[19] Ferrari R 1990 *Phys. Rev.* B **42** 4598
For an example of application of the Ferrari basis see Silberbauer H 1992 *J. Phys. Condens.: Matter* **4** 7355
[20] Brown E 1964 *Phys. Rev.* **133** A1038
Zak J 1964 *Phys. Rev.* **134** A1602
Zak J 1964 *Phys. Rev.* **134** A1607
[21] Schellnhuber H-J and Obermair G 1980 *Phys. Rev. Lett.* **45** 276
Obermair G M and Schellnhuber H-J 1981 *Phys. Rev.* B **23** 5185
Schellnhuber H-J, Obermair G M and Rauh A 1981 *Phys. Rev.* B **23** 5191
[22] Schellnhuber H-J 1982 *Phys. Rev.* B **25** 2358
[23] Anisimovas E and Johansson P 1999 *Phys. Rev.* B **60** 7744
[24] Chang M-C and Niu Q 1996 *Phys. Rev.* B **53** 7010
[25] Springsguth D, Ketzmerick R and Geisel T 1997 *Phys. Rev.* B **56** 2036
[26] Hamermesh M 1989 *Group Theory and its Application to Physical Problems* (New York: Dover) chapter 12
[27] Almbladh C-O 1999 private communication
Different variations of this technique are commonly used in band-structure calculations
[28] Dana I, Avron Y and Zak J 1985 *J. Phys. C: Solid State Phys.* **18** L679
Niu Q, Thouless D J and Wu Y-S 1985 *Phys. Rev.* B **31** 3372